

Increased detection of human cardiac troponin I by a decrease of nonspecific adsorption in diluted self-assembled monolayers

Jun Ren[†], Xiuqing Ding[†], John J. Greer[†] and Karthik Shankar[‡]

[†]Department of Physiology, and Women's and Children's Health Research Institute
Katz Group Centre for Pharmacy and Health Research, University of Alberta, Edmonton,
AB

[‡]Department of Electrical & Computer Engineering
W2-083 ECERF, University of Alberta, Edmonton, AB T6G 2V4.

Email address for correspondence : kshankar@ualberta.ca

ABSTRACT

In this paper, we tested the hypothesis that there is an increased sensitivity for detecting and measuring disease biomarkers (such as human cardiac troponin I, cTnI) by a decrease of nonspecific adsorption in diluted self assembled monolayers (SAMs) on planar sputtered gold films. Combining grazing angle Fourier-transform infrared spectroscopy (FT-IR) and antibody-antigen-antibody (sandwich) fluorescence-based immunoassay, we examined the relationship of sensitivity, specificity of detection of cTnI and the level of nonspecific protein adsorption in the following SAMs: pure MHA (16-mercaptohexadecanoic acid, 1 mM, with head COO⁻, $x=1.0$), a mixed SAM comprising MHA (0.1 mM) and UDT (1-undecane thiol, 0.9 mM, with hydrophobic head CH₃, $x=0.1_{UDT}$), and a mixed SAM comprising MHA (0.1 mM) and MUD (11-mercapto-1-undecanol, 0.9 mM, with hydrophilic head OH, $x=0.1_{MUD}$). Our data revealed that nonspecific binding to SAMs is favoured in the following order: CH₃ > COO⁻ > OH, consistent with previous studies. Compared with pure SAMs, diluting MHA SAMs with MUD increases the sensitivity of cTnI, whereas diluted MHA SAMs with UDT has the same sensitivity of detection of cTnI, suggesting it is the nature of the second diluting thiol that plays an important role on the amount of adsorbed protein on the surface. We obtained a 10-fold increase in the limit of detection of cTnI to 10 ng mL⁻¹ using $x=0.1_{MUD}$ due to a decrease of nonspecific binding. Further, specific binding between the antigen cTnI and its antibody is unaltered on pure and diluted SAMs.

KEYWORDS: nonspecific protein adsorption, immunoassay, ELISA, cardiac troponin I, 16-mercaptohexadecanoic acid, 1-undecane thiol, 11-mercapto-1-undecane, self assembled monolayer, gold film

1. INTRODUCTION

The development of surfaces resisting nonspecific protein adsorption has been an important subject for many biological and medical applications. Investigation of protein (disease biomarker) interactions in model systems such as enzyme linked immunosorbent assay (ELISA: antibody-antigen-antibody sandwich) are based on the specific interaction between protein in the bulk solution and capture probes attached to various types of

surfaces. In most cases, sensitivity is limited by the nonspecific adsorption of proteins, depending on the biophysical and chemical properties of the adsorbed surface. For ELISA, ~15% of measured response was estimated to be attributed to nonspecific protein/surface interactions[1]. Therefore, reducing non-specific adsorption is of paramount importance in immunosensor development.

Gold surfaces are commonly used substrates for the formation of well-ordered self-assembled monolayers (SAMs) and for most previous studies of protein adsorption, molecular recognition, and chemical and biological sensing. Alkanethiolates on gold, a well-established and widely studied SAM, forms densely packed, positionally constrained, and crystalline-like films in a very reproducible manner[2-5]. Although this high degree of order is important for certain applications, increasing attention is being given to mixed SAMs containing a diluted surface-active headgroup[6]. Greater control over the structure of the SAMs is afforded by coadsorption of two or more thiols that differ in the nature of the head group, tail group or the length of the hydrocarbon chain. Mixed SAMs generally have one thiolate with a functional headgroup at a low mole fraction and a second “spacer” thiolate at a high mole fraction[7]. Carboxylic acids are frequently chosen to be the functional headgroup because of their ability to bind to primary amines on the lysine residues of proteins to form stable amide bonds.

Close packed probe molecules are non-optimal for binding proteins due to molecular crowding resulting in steric hindrance[8]. In addition, irregular packing of primary antibodies in a sandwich-type assay bound to the SAM on the gold surface can prevent access to remaining active sites for the blocking agent following the analyte step and thus increase non-specific binding. Due to these factors, diluting the first thiol bearing the functional headgroups with a second thiol is useful in order to reduce the packing density of the probes, to prevent denaturation, minimize steric hindrance and thus improve the bioactivity of an immobilized protein[9-15].

Our objective in this work was to investigate whether there is an increased sensitivity for detecting and measuring disease biomarkers (such as human cardiac troponin I, cTnI) by a decrease of nonspecific adsorption in diluted SAMs. cTnI is a protein subunit of cardiac troponin complex. During the myocardial damage process, the troponin complex is broken up, and cTnI is released into the bloodstream. Because of this high tissue specificity and related sensitivity, cTnI has become a cornerstone in the diagnosis of myocardial infarction[16]. Early detection of the protein marker cTnI in patients with acute coronary syndromes can predict the risk of death[17]. Most cTnI assays are currently based on the conventional ELISA and have a detection limit of ~1 ng/ml. Highly sensitive and selective diagnostic assays have been achieved based on self-assembled monolayers, with a detection of one to seven orders of magnitude lower than those detected by ELISA[18-21]. Previous studies have examined how different types of functional groups can affect the amount of adsorbed protein at surfaces. This study examines how different surface coverage and the nature of the diluting SAMs of functional groups can affect adsorbed proteins on the surface, taking the cTnI sandwich as a model system. A schematic of the assay configuration is shown in **Figure 1**.

2. EXPERIMENTAL DETAILS

2.1 Materials.

1-undecane thiol (UDT), 11-mercapto-1-undecanol (MUD), 16-mercaptohexadecanoic acid (MHA), 1-ethyl-3-(3-dimethylaminopropyl) carbodiimide hydrochloride (EDC), N-hydroxysuccinimide (NHS), bovine serum albumin (BSA), and anhydrous ethanol were purchased from Sigma/Aldrich, USA. Phosphate buffered saline (PBS, pH 7.4) was used as the working medium (Sigma). Human cardiac troponin I (cTnI, #30-AT43), goat anti-cTnI (capture antibody for forming functional surface assembly, #70-TG004), mouse anti-cTnI (detection antibody, #10-T79B), mouse anti-skeletal muscle troponin I (anti-sTnI; #10R-T126A) were purchased from Fitzgerald Industries International, Inc (MA, USA). IR 680 (IRdye 680LT conjugated goat anti-mouse IgG) was purchased from the Li-cor Biosciences, Nebraska, USA). Unless otherwise stated, all chemicals used in this study were of analytical grade.

2.2 Functional Surface Assembly.

The Au substrates were prepared on silicon wafers by sputtering of 50-Å Cr and 1000-Å Au. The Au surfaces were immersed in the different thiols for 7 days: 1) solution of MHA (1 mM, with head-group COOH) alone, 2) mixed solution of MHA (0.1 mM) and UDT (0.9 mM, with head-group CH₃), and 3) mixed solution of MHA (0.1 mM) and MUD (0.9 mM, with head-group OH). In this study, we named these varied SAMs: pure MHA ($x=1.0$), a mixed SAM comprising MHA and UDT with a ratio of 1:9 ($x=0.1_{\text{UDT}}$), a mixed SAM comprising MHA and MUD with a ratio of 1:9 ($x=0.1_{\text{MUD}}$). After SAM formation, the resulting samples were washed with ethanol, distilled water and dried under nitrogen. In general, the ratio of the concentration of the two components in a mixed monolayer may be not the same as in solution but reflects the relative solubility of the components in solution and the interactions between the tail groups in the monolayers[22], but was assumed close to the solution composition in the present study, a reasonable assumption for these very similar molecules[23]. Activated esters of the carboxy terminii on MHA were subsequently formed by adding 100 mM EDC and 50 mM NHS in distilled water to SAMs for 1 h, followed by a wash with PBS. A 20 µg/ml solution of goat anti-cTnI in PBS was then added for 1 h to form an amide bond between the primary amine on anti-cTnI and the activated esters of the carboxy termini on MHA, followed by washing with PBS to rinse out the unbound excess anti-cTnI.

2.3 Apparatus

The XPS measurements were performed on an AXIS ULTRA spectrometer (Kratos Analytical Ltd. UK). The base pressure in the analytical chamber was lower than 2×10^{-7} Pa. The resolution function of the instrument for Al-mono source, hybrid lens mode is 0.7 eV for Au 4f peaks. Monochromated Al Ka ($h\nu=1486.6$ eV) was used at a power of 210 Watts. Fixed analyser transmission (FAT) mode was applied. The analysis spot was 700×400 µm. Charge neutralization was not required. All survey scans spanned from 1100 to 0 eV binding energy and were collected with analyzer pass energy (PE) of 160 eV with a step of 0.35 eV. For the high-resolution spectra, the pass-energy was 20 eV with a step of 0.1 eV.

Grazing angle Fourier-transform infrared spectroscopy (FT-IR) was performed at using a Thermo Nicolet 8700 infrared spectrometer via reflectance using IR light incident

at 85-86.5°. Spectra are the result of 1024 scans. A blank gold substrate spectrum, scanned under identical conditions, was used for background subtraction. The fluorescence signal was detected by using a Zeiss upright epi-fluorescence microscope (Axioskop 2 mot plus, Germany). A mercury arc lamp was used as the light source with the appropriate set of filters for the dyeexcitation and emission wavelengths. A Zeiss 12-bit cooled CCD camera (AxioCam MRc5, Germany) operated with Auxiovision software was used to acquire images at an exposure time of 2 s.

2.4 Antibody-Antigen-Antibody Immobilization and Fluorescent Detection Principle and Data Processing.

After binding with goat anti-cTnI, remaining active sites on the functional SAM were then blocked with 1% bovine serum albumin (BSA), followed by washing with PBS to rinse out the unbound excess BSA. This BSA step aims at blocking fractions of the surface that are not covered with anti-cTnI to prevent non-specific binding to the monolayer. Since cTnI will not bind to a BSA layer and BSA does not associate with anti-cTnI, the blocking step is expected to ensure cTnI immobilization strictly to anti-cTnI. Subsequently, various concentrations of cTnI were added for 1 hour, followed by washing with PBS to rinse out the unbound cTnI. Detection antibody mouse anti-cTnI was then added for 1 hour and followed by washing with PBS to rinse out the unbound anti-cTnI. Finally, fluorescent IR680 was added for one hour incubation and followed by washing with PBS to rinse out the unbound IR680. The amount of fluorescence signal is dependent on the amount of mouse anti-cTnI-IR680 bound on cTnI, thus the concentration of cTnI bound to goat anti-cTnI in the functional SAMs. In control experiments (cTnI=0), all steps were identical, except that the cTnI incubation step was replaced with PBS. The intensity of fluorescence over the whole surface of each slide was analyzed with histogram by Image-Pro Plus (Media Cybernetics, Silver Spring, MD, USA). The mean fluorescence intensity in each slide was a raw number, without subtracting the mean intensity obtained for the control. Data are displayed as mean \pm SEM, and Sigmaplot 11 (Systat software, San Jose, CA) is used for statistics analysis. T-test and one way ANOVA are used to compare two groups and multiple groups for significant differences, respectively, with $p < 0.05$ as a significant difference.

3. RESULTS AND DISCUSSION

3.1 XPS characterization of gold surfaces

XPS technique has been used to analyze the chemical composition of the material surfaces before and after chemical modifications to evaluate the nature of the chemical bonding occurring on the surface. The XPS survey scans (**Figure 2A**) detected gold for all Au surfaces examined, with the Au4f peaks appeared at 83.8 eV and 87.6 eV. After formation of SAM onto Au, S2p peaks were observed at 161.8 eV and 163.2 eV for a SAM-Au (**Figure 2B**), while no S2p peak is observed in the survey spectra of blank Au-silicon. This binding energy is characteristic to the chemical state of the S2p_{3/2} in the gold-thiol bond, consistent with previously published result[24]. Thus, the above result indicates that MHA was chemisorbed on Au-silicon through Au-S bonding and so the -COOH groups are exposed at the surface side in the SAMs[25].

3.2 FT-IR characterization of gold surfaces.

Each step of the surface modification process could be monitored by p-polarized grazing angle FT-IR. There are two characteristic diagnostic peaks, with one occurring at 1500-1850 cm^{-1} and the other at 2800-3000 cm^{-1} . We first examined the IR spectra of the various SAMs ($x=1.0$, $x=0.1_{\text{UDT}}$, $x=0.1_{\text{MUD}}$) at 2800-3000 cm^{-1} . There are two features around 2850 and 2940 cm^{-1} for $x=1.0$ and $x=0.1_{\text{UDT}}$, assigned to the CH_2 symmetric and CH_2 asymmetric modes from the carbon backbone, respectively. The IR spectrum shows that there are four vibrational modes around 2855, 2875, 2940, 2960 cm^{-1} for $x=0.1_{\text{MUD}}$. They are assigned to the CH_2 symmetric stretch, CH_3 symmetric stretch, CH_2 asymmetric stretch, and CH_3 asymmetric stretch modes, respectively. The peaks at 2850 and 2940 cm^{-1} were no difference among diluted SAMs ($x=0.1_{\text{MUD}}$ or $x=0.1_{\text{UDT}}$), but higher in $x=1$ SAMs.

We then focus the IR spectra on the C=O stretching region (1500-1850 cm^{-1} , **Figure 3**) of the spectrum, since this region is most diagnostic for the changes that occur during activation of the carboxylic acid group and formation of the amide bond[23]. The IR spectrum (**Fig. 3a**) obtained from all three SAMs shows the peak around 1740 cm^{-1} , which is related to the COOH moieties. The peaks were no difference between $x=0.1_{\text{MUD}}$ or $x=0.1_{\text{UDT}}$ SAMs, but ~60% higher in $x=1$ than $x=0.1_{\text{MUD}}$ or $x=0.1_{\text{UDT}}$ SAMs. This is consistent with a previous report[23]. Reaction with EDC and NHS produced a SAM with characteristic peaks at 1815, 1750, and 1700 cm^{-1} , which are responsible for the carbonyl stretch modes in the COO-NHS ester moiety. These peaks were no difference between $x=0.1_{\text{MUD}}$ or $x=0.1_{\text{UDT}}$ SAMs, but ~25% higher in $x=1$ than $x=0.1_{\text{MUD}}$ or $x=0.1_{\text{UDT}}$ SAMs (**Fig. 3b**). These results suggest that successful formation of the ester intermediate depends on the accessibility of the terminal carboxylate groups. Steric packing of these acid groups in pure SAMs can limit the rate and capacity of intermediate formation, with partial conversion (~50%) of accessible acid groups occurring only after first reaction cycle[26]. After anti-cTnI immobilization new amide bands appeared around 1670 and 1550 cm^{-1} (amide I and amide II), indicating the existence of anti-cTnI on the surface (**Fig. 3c**). We assign the band at 1550 cm^{-1} to the two NH bends, the band at 1670 cm^{-1} to the two amide C=O stretches in the coupled ligand, and the band at 1730 cm^{-1} to the C=O stretch of residual carboxylic acid groups in MHA. These results were similar to that of previous studies[23, 26], suggesting formation of functional SAMs. Whereas the peak of two amide bands was not different among all SAMs, the band at 1730 cm^{-1} was smaller in both diluted SAMs than non-diluted SAMs. Moreover, 1 of 4 SAMs in $x=0.1_{\text{UDT}}$, and 2 of 4 SAMs in $x=0.1_{\text{MUD}}$ had no detectable band at 1730 cm^{-1} , indicating less residual carboxylic acid groups in diluted MHA. Further incubation with BSA (1%, **Fig. 3d**) after anti-cTnI revealed that $x=1$ SAMs had a ~20% increase in the peak of the primary amide band at 1670 cm^{-1} , 30% decrease in the band at 1730 cm^{-1} . Further incubation with BSA after anti-cTnI revealed that diluted SAMs had a ~5% increase at 1670 cm^{-1} , 50% decrease in the band at 1730 cm^{-1} .

3.3 Fluorescence detection of cTnI.

First, we compared nonspecific binding capability in varied SAMs without NHS/EDC activation by measuring fluorescent labelling (**Figure 4**). Without pretreatment of BSA, fluorescent labelling by incubation of IR680 had readings of 210 ± 29 , 288 ± 26 , 101 ± 12 for $x=1$, $x=0.1_{\text{UDT}}$, $x=0.1_{\text{MUD}}$, respectively. After BSA

incubation, fluorescent labelling by incubation of IR680 was 42, 27, ~0 for $x=1$, $x=0.1_{\text{UDT}}$, $x=0.1_{\text{MUD}}$, respectively. These results were consistent with previous studies of the nonspecific binding of IgG and BSA to gold surfaces. The surface concentration of IgG and BSA molecules adsorbed on the SAMs revealed that nonspecific binding to SAMs is favoured in the following order: $\text{CH}_3 > \text{COO}^- > \text{NH}_3^+ > \text{OH} > \text{ethylene glycol}$ [27-29]. Prime & Whitesides (1991) showed that surfaces resisting adsorption of proteins exhibited four common molecular-level features: hydrophilic, electrically neutral, hydrogen bond acceptors, and not hydrogen bond donors[30]. For example, less bound water molecules around chains and lower chain flexibility, the lack of any hydrogen-bonding capability due to its nonpolar nature are major factors for protein adsorption on the CH_3 -SAM surface[31]. These results indicated the least amount of nonspecific binding of anti-IgG to $x=0.1_{\text{MUD}}$ SAMs. Most importantly, BSA fully occupied the nonspecific binding sites of $x=0.1_{\text{MUD}}$ SAMs, thus, BSA completely blocked nonspecific binding of fluorescent anti-IgG to $x=0.1_{\text{MUD}}$. BSA has 60 surface lysine groups that can have electrostatic interactions with negatively charged moieties. BSA can be conjugated to other proteins and peptides utilizing the large number of surface lysine residues of BSA as a scaffold for chemical attachment[32-34].

Secondly, after NHS/EDC activation, we compared fluorescent labelling by directly adding IR680 to various SAMs (**Figure 5**). Without pretreatment of BSA, fluorescent labelling capacity by incubation of IR680 was 1313 ± 88 , 1258 ± 79 , 1189 ± 76 for $x=1$, $x=0.1_{\text{UDT}}$, $x=0.1_{\text{MUD}}$ SAMs, respectively. There was no significant difference among them, suggesting two opposite possibilities: 1) similar amount of COO-NHS binding sites, 2) greater number of COO-NHS binding sites in pure SAMs, but with low binding efficacy. Our FT-IR data supported the second possibility, as evidenced by the fact that the peaks of COO-NHS ester moiety were higher in $x=1$ than $x=0.1$ SAMs. But more residual carboxylic acid groups were found after anti-cTnI or BSA incubation in $x=1$ than $x=0.1$ SAMs. Only a fraction of COO-NHS binding sites form the covalent amino binding because IR680 is a huge molecule. The layer containing the highest amount of COO-NHS ester was the least efficient in terms of fluorescent IR680 binding capacity.

After incubation of BSA, fluorescent labelling by incubation of IR680 was 186 ± 15 , 101 ± 13 , 55 ± 12 , for $x=1$, $x=0.1_{\text{UDT}}$, $x=0.1_{\text{MUD}}$, respectively. The smaller the number, the fewer non-specific binding sites left for IR680. These results suggested that $x=0.1_{\text{MUD}}$ had most physical nonspecific and chemical specific binding sites bound by BSA. As discussed above, this result is consistent with previous studies of the surface concentration of IgG and BSA molecules adsorbed on the SAMs[29]. The kinetics of the binding curves for the adsorption of the proteins are described in terms of multiple states of adsorbed proteins that involve multipoint hydrophobic, electrostatic, hydrogen bond, and amide bond interactions for the different surfaces and protein lateral interactions caused by the unfolding of adsorbed proteins. Further testing of diluted MHA in MUD (1:50; $x=0.02_{\text{MUD}}$) found that fluorescence count was ~350, and after BSA blocking, the count was ~20, suggesting a similar favoured ratio as that observed in $x=0.1_{\text{MUD}}$. Steric effects are reduced when the reactive site is tethered to a molecular component of a mixed SAM that is longer than those comprising the surrounding organic background[23].

Next, the fluorescent images were taken after the goat anti-cTnI, BSA, cTnI (5-100 ng/ml), mouse anti-cTnI, and fluorescent IR680 steps (**Figure 6**). For the negative control samples, all the same steps were taken excepting replacement of cTnI by PBS. For $x=1$ SAMs, the control fluorescence count was 310 ± 80 , whereas cTnI (100 ng/ml) was detected with a fluorescent number of 705 ± 117 ($p<0.01$, $n=5$). However, the cTnI (50 ng/ml) was not detected (485 ± 78 , $p>0.05$, $n=5$). For $x=0.1_{\text{UDT}}$ SAMs, the control reading was at 282 ± 51 , whereas cTnI (100 ng/ml) was detected with a fluorescent number of 672 ± 91 ($p<0.01$, $n=5$). However, the cTnI (50 ng/ml) was not detected (414 ± 73 , $p>0.05$, $n=5$). For $x=0.1_{\text{MUD}}$ SAMs, the control fluorescence was at 92 ± 15 , whereas cTnI (10, 50, 100 ng/ml, $n=5$ each) was detected with a fluorescent number of 201 ± 34 ($p<0.05$), 479 ± 84 ($p<0.001$), 603 ± 88 ($p<0.001$), respectively. For $x=0.1_{\text{MUD}}$, cTnI (5 ng/ml, $n=5$) had a fluorescent number of 132 ± 23 , not significantly different from the control ($p>0.05$). These results combined with FT-IR observation suggested that the sensitivity of the optimum sensor surface may not correspond to the highest density of immobilized antibody, consistent with the conclusion of previous studies[35, 36].

Compared with pure MHA SAMs, diluted MHA SAMs with MUD (hydrophilic head) increases the sensitivity of cTnI, whereas diluted MHA SAMs with UDT (hydrophobic head) does not have a different sensitivity to cTnI. Our results further demonstrated it is the nature of the second thiol that plays an important role on the amount of adsorbed protein at surface. ~ 10 times of increased detection of cTnI using $x=0.1_{\text{MUD}}$ is due to a decrease of nonspecific binding, whereas binding capacity at high concentration of cTnI (100 ng/ml) was no different among the varied SAMs. Note that the lowest detection level of 10 ng/ml cTnI with fluorescent labelling in this study is much higher than that detected by commercial ELISA kits and nano biosensors. It is probably due to the following: 1) limitation of fluorescent detection by IR680; 2) all the process steps including forming functional anti-cTnI SAMs, cTnI, anti-cTnI, fluorescent IR680 need thoroughly shaking to fully react and thoroughly washout. Because of the nature of flat surface and expensive chemicals, all these reactions were carried on the still surface without thoroughly shaking; 3) most importantly, we did not employ the amplification step (outside the scope of this study).

Even though the number of active sites is significantly decreased in the diluted mixed monolayer method, therefore potentially limiting sensitivities, we found the lower limit of detection and reproducibility of the assay to actually improve due to the reduction of non-specific binding. The increased acidity of the diluted carboxylic acid groups and better control over the availability and orientation of epitopes may also play a role. A downside to mixed monolayers is the possibility of deleterious phase segregation between the two components of the binary SAM resulting in individual domains comprised purely of one component, which eliminates some of the advantages of using mixed monolayers[37]. Phase segregation is maximum when the two components differ greatly in chain-length, are present in the the monolayer adsorption solution in comparable concentrations and when the head-groups corresponding to the two components are most unlike each other (e.g. hydrophobic and hydrophilic headgroups). Even in such extreme cases[38-41], domain sizes of only $\sim 15 \text{ nm}^2$ have been observed, which is comparable to the size of the proteins used (antitroponin and troponin)[42]. Using scanning probe microscopy, Weiss and colleagues observed nanoscale phase separation in mixed SAMs of $\text{CH}_3(\text{CH}_2)_{15}\text{SH}$ and $\text{CH}_3\text{O}_2\text{C}(\text{CH}_2)_{15}\text{SH}$ with domain sizes

less than 2.5 nm in diameter[43]. Since the headgroups in the two components used by us are both hydrophilic, the concentration of the surface-active component is only 10% of the overall mixture, and because the difference in chain length is only 5 carbon atoms, we expect domains to be significantly smaller than proteins in our binary SAMs. While employing components with alkyl chains of equal or very similar lengths is helpful toward achieving a perfectly random mixed monolayer, minimizing phase segregation is not the only objective. Another objective is to minimize biofouling and for this purpose, embedding a longer chain surface-active component in a shorter chain non-fouling background has been shown to be effective[44], which our results strongly support.

3.4 Antigen recognition

It is well known that proteins and antibodies adsorbed on a surface may lose part of their bioactivity due to conformational changes and/or nonoptimal orientation and distribution on the surface[29, 35, 45]. One study[46] indicated that at higher probe densities, functional SAMs are unable to discriminate between its specific antibody and non-specific antibodies, and only diluted SAMs with lower surface coverage prevent nonspecific binding between an antigen and its antibody. A survey of structure-property relationships of surfaces revealed those nonadsorbing thiolates, which resisted the adsorption of proteins, were hydrophilic and electrically neutral and contained groups that were hydrogen-bond acceptors but not hydrogen-bond donors[47, 48]. This raised an issue of great importance: whether specific binding between an antigen and its antibody depended on the surface coverage. In this study, we tested a molecule with a similar structure of anti-cTnI, anti-skeletal muscle troponin I (anti-sTnI) in both $x=1$ and $x=0.1_{\text{MUD}}$ SAMs with all identical steps, except that in the detection step, anti-cTnI (20 $\mu\text{g/ml}$) was replaced by anti-sTnI (20 $\mu\text{g/ml}$) or PBS only (**Figure 7**). In $x=1$ SAMs, the fluorescent labelling by anti-sTnI was 287 ± 71 , no different from 310 ± 80 in PBS control ($p>0.05$), significantly smaller than 705 ± 117 in samples with a detection anti-cTnI ($p<0.01$). In $x=0.1_{\text{MUD}}$ SAMs, the fluorescent labelling by anti-sTnI was 116 ± 38 , no different from 92 ± 15 in PBS control ($p>0.05$), significantly smaller than 672 ± 91 in samples with a detection anti-cTnI ($p<0.01$). These results suggest that cTnI specifically binds only to detection anti-cTnI, and not to anti-sTnI whether pure ($x=1$) or diluted ($x=0.1_{\text{MUD}}$) MHA SAMs are used. Specific binding between the cTnI and its antibody is unaltered on pure and mixed SAMs.

4. CONCLUSIONS

This study has proved that different surface coverage and the nature of the diluting SAMs can affect the amount of adsorbed protein at surface, taking the cTnI sandwich as a model system. For mixed SAMs having one thiolate with a functional headgroup (like a carboxylic acid) at a low mole fraction and second thiolate at a high mole fraction, the nature of the second thiol decides the amount of adsorbed protein at surface. Compared with pure MHA SAMs, diluted MHA SAMs with MUD (hydrophilic head) increases the sensitivity of detection of cTnI, whereas diluted MHA SAMs with UDT (hydrophobic head) does not change the sensitivity of detection of cTnI. Increased detection of cTnI is due to decreased nonspecific adsorption. Specific binding between the antigen cTnI and its antibody is unaltered on pure and diluted SAMs.

The principle of increased recognition of cTnI by decrease of nonspecific adsorption in mixed SAMs diluted by a second thiol with a hydrophilic head-group could be used for enhanced detection of other important disease biomarkers. Although these studies were performed using immunolabeling, the strategy of enhanced detection of proteins in diluted SAMs with second thiol with hydrophilic head should also be useful in conjunction with other analytical techniques.

ACKNOWLEDGEMENTS

We would like to thank Ni Yang at Oil Sands and Coal Interfacial Engineering Facility and Wayne Moffat in the Department of Chemistry for assistance with FT-IR, and Drs. Dimitre Karpuzov, Anquang He and Shihong Xu at the Alberta Centre for Surface Engineering and Science for assistance with XPS measurements. K.S. thanks NSERC and CFI for funding support.

REFERENCES

- [1] J. Renken, R. Dahint, M. Grunze, F. Josse, Multifrequency evaluation of different immunosorbents on acoustic plate mode sensors, *Anal. Chem.*, 68 (1996) 176-182.
- [2] C.D. Bain, E.B. Troughton, Y.T. Tao, J. Evall, G.M. Whitesides, R.G. Nuzzo, Formation of monolayer films by the spontaneous assembly of organic thiols from solution onto gold, *J. Am. Chem. Soc.*, 111 (1989) 321-335.
- [3] R.G. Nuzzo, L.H. Dubois, D.L. Allara, Fundamental-studies of microscopic wetting on organic-surfaces. 1. Formation and structural characterization of a self-consistent series of polyfunctional organic monolayers, *J. Am. Chem. Soc.*, 112 (1990) 558-569.
- [4] G.M. Whitesides, P.E. Laibinis, Wet chemical approaches to the characterization of organic-surfaces - self-assembled monolayers, wetting, and the physical organic-chemistry of the solid liquid interface, *Langmuir*, 6 (1990) 87-96.
- [5] N. Sandhyarani, T. Pradeep, Characteristics of alkanethiol self assembled monolayers prepared on sputtered gold films: a surface enhanced Raman spectroscopic investigation, *Vacuum*, 49 (1998) 279-284.
- [6] J. Lahann, S. Mitragotri, T.N. Tran, H. Kaido, J. Sundaram, I.S. Choi, S. Hoffer, G.A. Somorjai, R. Langer, A reversibly switching surface, *Science*, 299 (2003) 371-374.
- [7] D.R. Shankaran, N. Miura, Trends in interfacial design for surface plasmon resonance based immunoassays, *J. Phys. D-Appl. Phys.*, 40 (2007) 7187-7200.
- [8] A. Vaish, M.J. Shuster, S. Cheunkar, P.S. Weiss, A.M. Andrews, Tuning Stamp Surface Energy for Soft Lithography of Polar Molecules to Fabricate Bioactive Small-Molecule Microarrays, *Small*, 7 (2011) 1471-1479.
- [9] F. Frederix, K. Bonroy, W. Laureyn, G. Reekmans, A. Campitelli, W. Dehaen, G. Maes, Enhanced performance of an affinity biosensor interface based on mixed self-assembled monolayers of thiols on gold, *Langmuir*, 19 (2003) 4351-4357.
- [10] B. Ge, F. Lisdat, Superoxide sensor based on cytochrome c immobilized on mixed-thiol SAM with a new calibration method, *Anal. Chim. Acta*, 454 (2002) 53-64.
- [11] A.J. Guiomar, J.T. Guthrie, S.D. Evans, Use of mixed self-assembled monolayers in a study of the effect of the microenvironment on immobilized glucose oxidase, *Langmuir*, 15 (1999) 1198-1207.

- [12] S. Herrwerth, W. Eck, S. Reinhardt, M. Grunze, Factors that determine the protein resistance of oligoether self-assembled monolayers - Internal hydrophilicity, terminal hydrophilicity, and lateral packing density, *J. Am. Chem. Soc.*, 125 (2003) 9359-9366.
- [13] S. Herrwerth, T. Rosendahl, C. Feng, J. Fick, W. Eck, M. Himmelhaus, R. Dahint, M. Grunze, Covalent coupling of antibodies to self-assembled monolayers of carboxy-functionalized poly(ethylene glycol): Protein resistance and specific binding of biomolecules, *Langmuir*, 19 (2003) 1880-1887.
- [14] D. Hobara, T. Sasaki, S. Imabayashi, T. Kakiuchi, Surface structure of binary self-assembled monolayers formed by electrochemical selective replacement of adsorbed thiols, *Langmuir*, 15 (1999) 5073-5078.
- [15] M. Wirde, U. Gelius, L. Nyholm, Self-assembled monolayers of cystamine and cysteamine on gold studied by XPS and voltammetry, *Langmuir*, 15 (1999) 6370-6378.
- [16] J.E. Adams, G.S. Bodor, V.G. Davilaroman, J.A. Delmez, F.S. Apple, J.H. Ladenson, A.S. Jaffe, Cardiac troponin-I - A marker with high specificity for cardiac injury, *Circulation*, 88 (1993) 101-106.
- [17] E.M. Antman, M.J. Tanasijevic, B. Thompson, M. Schactman, C.H. McCabe, C.P. Cannon, G.A. Fischer, A.Y. Fung, C. Thompson, D. Wybenga, E. Braunwald, Cardiac-specific troponin I levels to predict the risk of mortality in patients with acute coronary syndromes, *N. Engl. J. Med.*, 335 (1996) 1342-1349.
- [18] L.R. Hirsch, J.B. Jackson, A. Lee, N.J. Halas, J. West, A whole blood immunoassay using gold nanoshells, *Anal. Chem.*, 75 (2003) 2377-2381.
- [19] J.S. Park, M.K. Cho, E.J. Lee, K.Y. Ahn, K.E. Lee, J.H. Jung, Y.J. Cho, S.S. Han, Y.K. Kim, J. Lee, A highly sensitive and selective diagnostic assay based on virus nanoparticles, *Nat. Nanotechnol.*, 4 (2009) 259-264.
- [20] N.L. Rosi, C.A. Mirkin, Nanostructures in biodiagnostics, *Chem. Rev.*, 105 (2005) 1547-1562.
- [21] J.T. Liu, C.J. Chen, T. Ikoma, T. Yoshioka, J.S. Cross, S.J. Chang, J.Z. Tsai, J. Tanaka, Surface plasmon resonance biosensor with high anti-fouling ability for the detection of cardiac marker troponin T, *Anal. Chim. Acta*, 703 (2011) 80-86.
- [22] C.D. Bain, G.M. Whitesides, Formation of 2-component surfaces by the spontaneous assembly of monolayers on gold from solutions containing mixtures of organic thiols, *J. Am. Chem. Soc.*, 110 (1988) 6560-6561.
- [23] J. Lahiri, L. Isaacs, J. Tien, G.M. Whitesides, A strategy for the generation of surfaces presenting ligands for studies of binding based on an active ester as a common reactive intermediate: A surface plasmon resonance study, *Anal. Chem.*, 71 (1999) 777-790.
- [24] P.A. Johnson, R. Levicky, X-ray photoelectron spectroscopy and differential capacitance study of thiol-functional polysiloxane films on gold supports, *Langmuir*, 20 (2004) 9621-9627.
- [25] F. Nakamura, E. Ito, T. Hayashi, M. Hara, Fabrication of COOH-terminated self-assembled monolayers for DNA sensors, *Colloid Surf. A-Physicochem. Eng. Asp.*, 284 (2006) 495-498.
- [26] B.L. Frey, R.M. Corn, Covalent attachment and derivatization of poly(L-lysine) monolayers on gold surfaces as characterized by polarization-modulation FT-IR spectroscopy, *Anal. Chem.*, 68 (1996) 3187-3193.

- [27] A.M. Moulin, S.J. O'Shea, R.A. Badley, P. Doyle, M.E. Welland, Measuring surface-induced conformational changes in proteins, *Langmuir*, 15 (1999) 8776-8779.
- [28] S. Nakata, N. Kido, M. Hayashi, M. Hara, H. Sasabe, T. Sugawara, T. Matsuda, Chemisorption of proteins and their thiol derivatives onto gold surfaces: Characterization based on electrochemical nonlinearity, *Biophys. Chem.*, 62 (1996) 63-72.
- [29] V. Silin, H. Weetall, D.J. Vanderah, SPR studies of the nonspecific adsorption kinetics of human IgG and BSA on gold surfaces modified by self-assembled monolayers (SAMs), *J. Colloid Interface Sci.*, 185 (1997) 94-103.
- [30] K.L. Prime, G.M. Whitesides, Self-assembled organic monolayers - model systems for studying adsorption of proteins at surfaces, *Science*, 252 (1991) 1164-1167.
- [31] H. Zheng, H. Okada, S. Nojima, S. Suye, T. Hori, Layer-by-layer assembly of enzymes and polymerized mediator on electrode surface by electrostatic adsorption, *Sci. Technol. Adv. Mater.*, 5 (2004) 371-376.
- [32] S.H. Brewer, W.R. Glomm, M.C. Johnson, M.K. Knag, S. Franzen, Probing BSA binding to citrate-coated gold nanoparticles and surfaces, *Langmuir*, 21 (2005) 9303-9307.
- [33] A.G. Tkachenko, H. Xie, D. Coleman, W. Glomm, J. Ryan, M.F. Anderson, S. Franzen, D.L. Feldheim, Multifunctional gold nanoparticle-peptide complexes for nuclear targeting, *J. Am. Chem. Soc.*, 125 (2003) 4700-4701.
- [34] H. Xie, A.G. Tkachenko, W.R. Glomm, J.A. Ryan, M.K. Brennaman, J.M. Papanikolas, S. Franzen, D.L. Feldheim, Critical flocculation concentrations, binding isotherms, and ligand exchange properties of peptide-modified gold nanoparticles studied by UV-visible, fluorescence, and time-correlated single photon counting spectroscopies, *Anal. Chem.*, 75 (2003) 5797-5805.
- [35] E. Briand, M. Salmain, J.M. Herry, H. Perrot, C. Compere, C.M. Pradier, Building of an immunosensor: How can the composition and structure of the thiol attachment layer affect the immunosensor efficiency?, *Biosens. Bioelectron.*, 22 (2006) 440-448.
- [36] M.L.M. Vareiro, J. Liu, W. Knoll, K. Zak, D. Williams, A.T.A. Jenkins, Surface plasmon fluorescence measurements of human chorionic gonadotrophin: Role of antibody orientation in obtaining enhanced sensitivity and limit of detection, *Anal. Chem.*, 77 (2005) 2426-2431.
- [37] Y. Arima, H. Iwata, Effect of wettability and surface functional groups on protein adsorption and cell adhesion using well-defined mixed self-assembled monolayers, *Biomaterials*, 28 (2007) 3074-3082.
- [38] N.J. Brewer, G.J. Leggett, Chemical force microscopy of mixed self-assembled monolayers of alkanethiols on gold: Evidence for phase separation, *Langmuir*, 20 (2004) 4109-4115.
- [39] D. Hobara, M. Ota, S. Imabayashi, K. Niki, T. Kakiuchi, Phase separation of binary self-assembled thiol monolayers composed of 1-hexadecanethiol and 3-mercaptopropionic acid on Au(111) studied by scanning tunneling microscopy and cyclic voltammetry, *J. Electroanal. Chem.*, 444 (1998) 113-119.
- [40] R. Schweiss, D. Pleul, F. Simon, A. Janke, P.B. Welzel, B. Voit, W. Knoll, C. Werner, Electrokinetic potentials of binary self-assembled monolayers on gold: Acid-base reactions and double layer structure, *J. Phys. Chem. B*, 108 (2004) 2910-2917.

- [41] R. Schweiss, P. Welzel, W. Knoll, C. Werner, Assembly modulates dissociation: electrokinetic experiments reveal peculiarities of the charge formation at monolayer films, *Chem. Commun.*, (2005) 256-258.
- [42] C.B. Anfinsen, J.T. Edsall, F.M. Richards, *Advances in Protein Chemistry*, in, Academic Press, 1986.
- [43] S.J. Stranick, A.N. Parikh, Y.T. Tao, D.L. Allara, P.S. Weiss, Phase-separation of mixed-composition self-assembled monolayers into nanometer-scale molecular domains, *J. Phys. Chem.*, 98 (1994) 7636-7646.
- [44] Q.M. Yu, S.F. Chen, A.D. Taylor, J. Homola, B. Hock, S.Y. Jiang, Detection of low-molecular-weight domoic acid using surface plasmon resonance sensor, *Sens. Actuator B-Chem.*, 107 (2005) 193-201.
- [45] W. Norde, Adsorption of proteins from solution at the solid-liquid interface, *Adv. Colloid Interface Sci.*, 25 (1986) 267-340.
- [46] M.J. Shuster, A. Vaish, M.E. Szapacs, M.E. Anderson, P.S. Weiss, A.M. Andrews, Biospecific recognition of tethered small molecules diluted in self-assembled monolayers, *Adv. Mater.*, 20 (2008) 164-+.
- [47] R.G. Chapman, E. Ostuni, S. Takayama, R.E. Holmlin, L. Yan, G.M. Whitesides, Surveying for surfaces that resist the adsorption of proteins, *J. Am. Chem. Soc.*, 122 (2000) 8303-8304.
- [48] E. Ostuni, R.G. Chapman, R.E. Holmlin, S. Takayama, G.M. Whitesides, A survey of structure-property relationships of surfaces that resist the adsorption of protein, *Langmuir*, 17 (2001) 5605-5620.

Figure Captions

Figure 1 Schematic of the diluted mixed monolayer approach toward reducing steric hindrance and non-specific binding in troponin assays

Figure 2 Survey XPS spectra of the gold surfaces after formation of MHA SAM on gold. Au4f peaks appeared at 83.8 eV and 87.6 eV (A); while S2p peaks were observed at 161.8 eV and 163.2 eV for a SAM-Au (B). The S2p peaks were not observed from bare gold.

Figure 3 The IR spectra of the various SAMs used in this study with a focus on the C=O stretching region ($1500\text{-}1850\text{ cm}^{-1}$) of the spectrum. Each step of the gold surface modification process could be monitored by p-polarized grazing angle FT-IR. Characteristic diagnostic peaks occurred between 1500 cm^{-1} and 1850 cm^{-1} . FT-IR spectra obtained for MHA SAMs on $x=1$, $x=0.1_{\text{UDT}}$, $x=0.1_{\text{MUD}}$, prior to (a), post (b) activation of the carboxylic acid group, followed by formation of the amide bond between the primary amine on anti-cTnI and the activated esters of the carboxy termini on MHA (c), and further BSA incubation (d).

Figure 4 Nonspecific binding capability in varied SAMs without NHS/EDC activation by measuring fluorescent labelling by directly adding IR680 to activated SAMs without or after BSA incubation. ^{NS} $p>0.05$: no significant difference between two compared groups; * $p<0.05$, ** $p<0.01$, *** $p<0.001$: significant difference between two compared groups. Each data point is 4 samples.

Figure 5 Binding capability in varied SAMs after NHS/EDC activation by measuring fluorescent labelling. Fluorescent labelling by directly adding IR680 to activated SAMs without or after BSA incubation. There is no significant difference in binding capabilities of IR680 to varied SAMs. * $p<0.05$, ** $p<0.01$: significant difference between compared groups. Each data point is 4 samples.

Figure 6 Detection of cardiac troponin I (cTnI) in varied SAMs by measuring fluorescent labelling. Representative fluorescent images were taken after the goat anti-cTnI (20 $\mu\text{g/ml}$), BSA, cTnI (10-100 ng/ml), mouse anti-cTnI (20 $\mu\text{g/ml}$), and fluorescent IR680 immunoassay for MHA SAMs on $x=1$ (A), $x=0.1_{\text{UDT}}$ (B), $x=0.1_{\text{MUD}}$ (C). Negative control (cTnI=0) was taken all the same steps except of replacement of cTnI by PBS. Each image is 0.7 cm X 0.7 cm. D) Population data. ^{NS} $p>0.05$: no significant difference compared with their own control; * $p<0.05$, ** $p<0.01$, *** $p<0.001$: significant difference compared with their own control. Each data point is 5 samples.

Figure 7 Binding specificity of cardiac troponin I (cTnI) in varied anti-cTnI functional SAMs by measuring fluorescent labelling. The fluorescent images were taken after the goat anti-cTnI (20 $\mu\text{g/ml}$), BSA, cTnI (100 ng/ml), mouse anti-cTnI (20 $\mu\text{g/ml}$) or anti-sTnI (20 $\mu\text{g/ml}$) or PBS only, and fluorescent IR680 immunoassay. ^{NS} $p>0.05$: no significant difference between two compared groups; ** $p<0.01$, *** $p<0.001$: significant difference between two compared groups. Each data point is 5 samples.

List of Figures

Figure 1

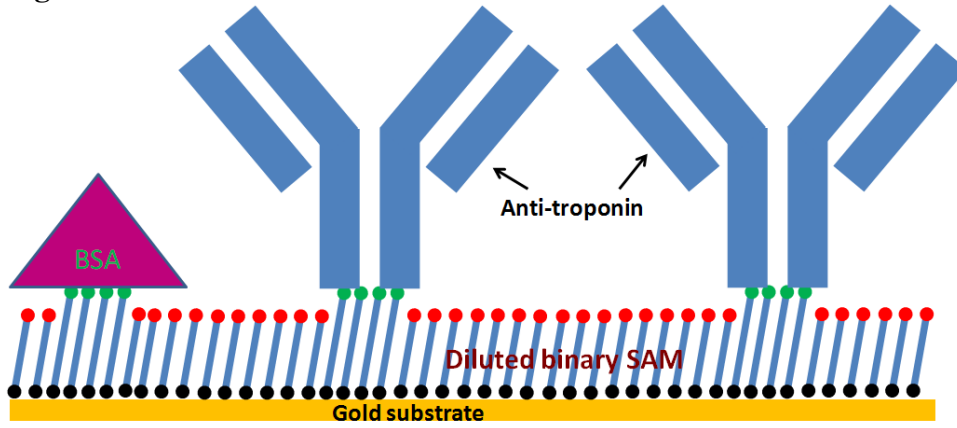


Figure 2

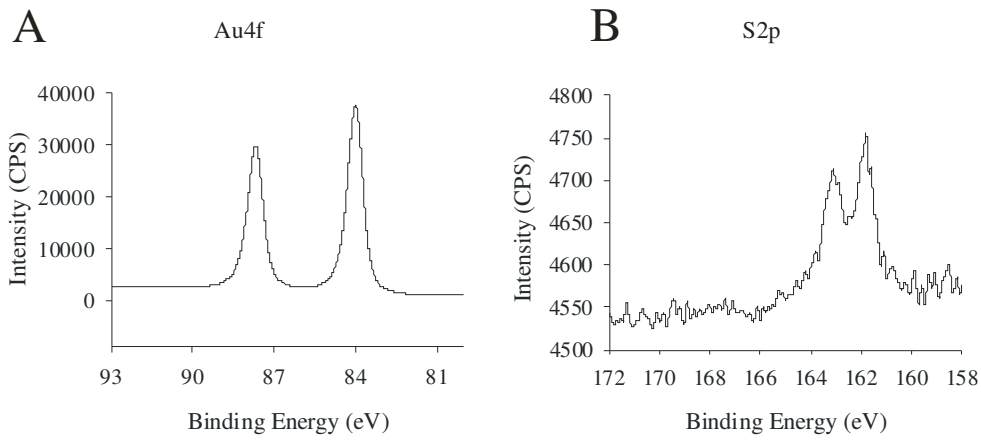


Figure 3

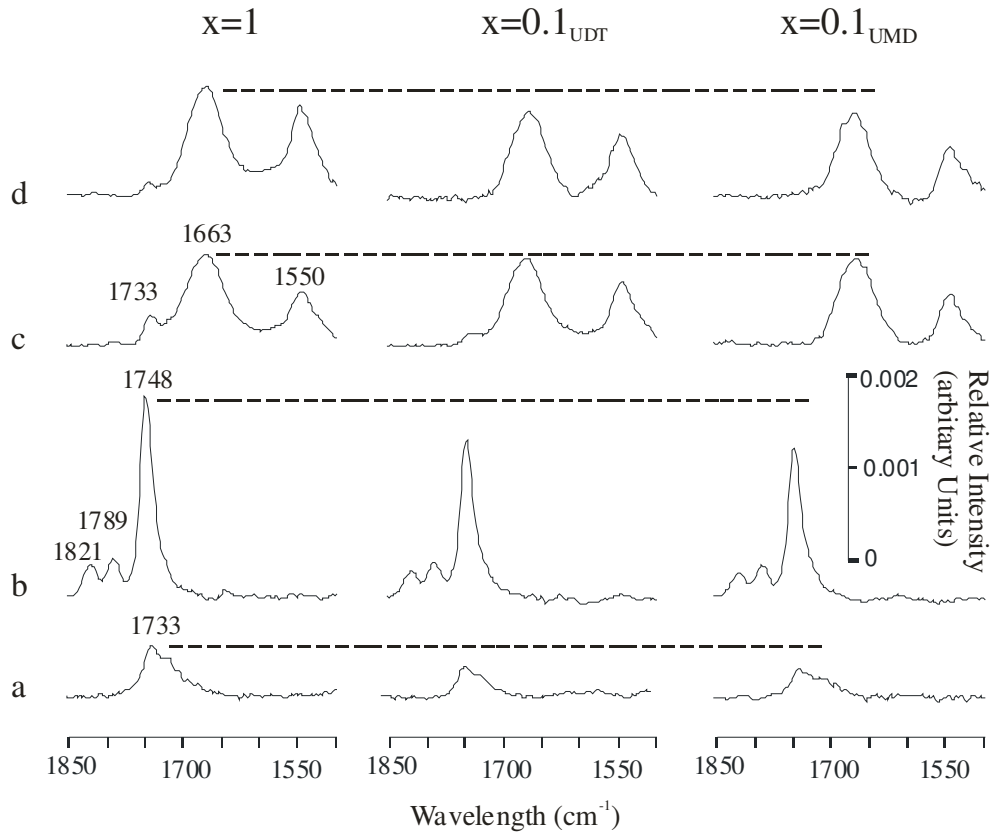


Figure 4

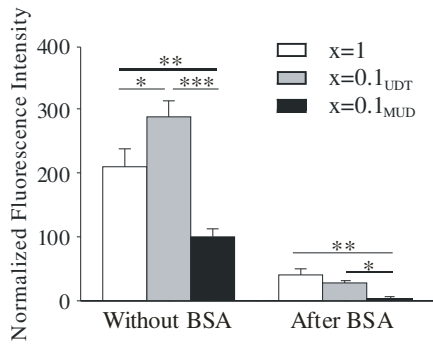


Figure 5

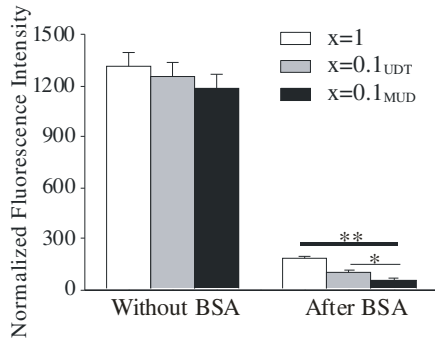


Figure 6

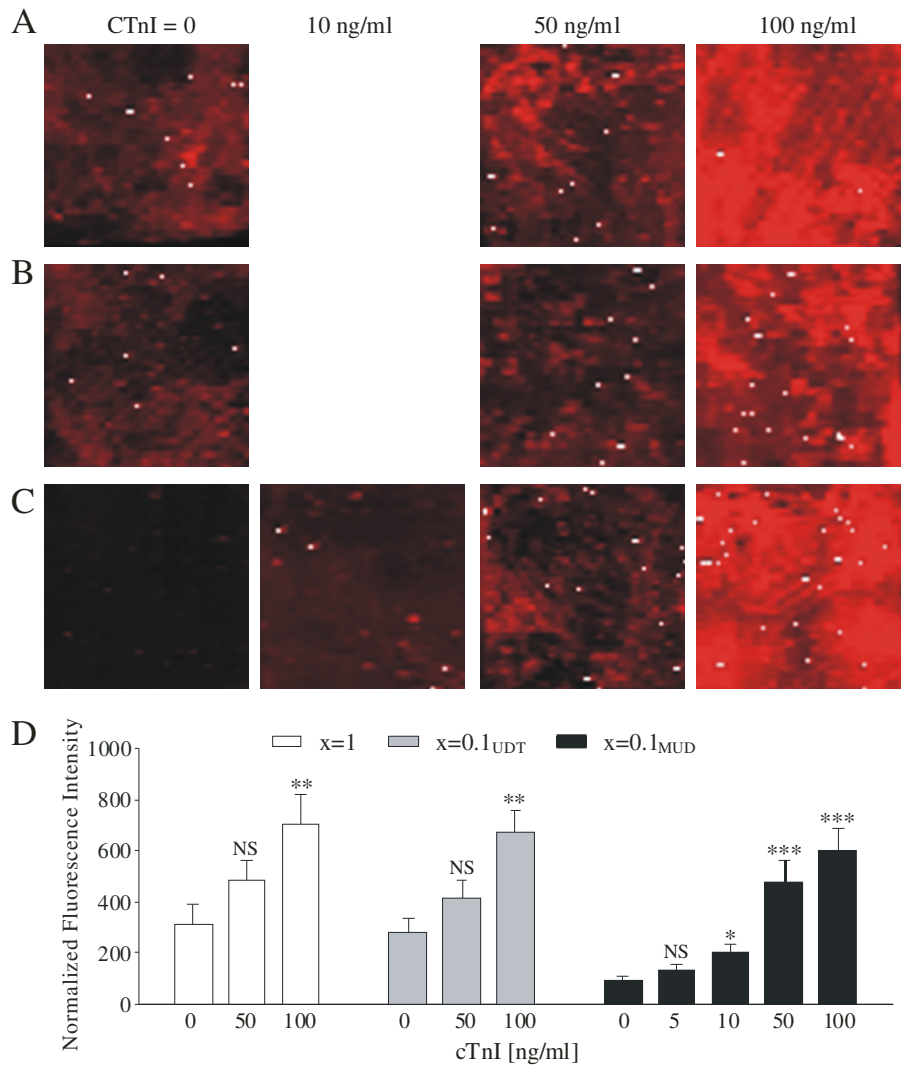


Figure 7

